Research Square

Preprints are preliminary reports that have not undergone peer review.
They should not be considered conclusive, used to inform clinical practice,
or referenced by the media as validated information.

Brain MRI evidence of distinct contiguous gene syndrome in 22q13 deletion-related disorders

Khawla Aljabali
Imagine Institute, Université Paris Cité, INSERM U1163
Aurelie Fabre
Imagine Institute, Université Paris Cité, INSERM U1163
Anne Philippe
Imagine Institute, Université Paris Cité, INSERM U1163
Jennifer Boisgontier
Imagine Institute, Université Paris Cité, INSERM U1163
Ludovic Fillon
Imagine Institute, Université Paris Cité, INSERM U1163
Ana Saitovitch
Imagine Institute, Université Paris Cité, INSERM U1163
Sara Cabet
Imagine Institute, Université Paris Cité, INSERM U1163
Volodia Dangouloff-Ros
Imagine Institute, Université Paris Cité, INSERM U1163
Marlene Rio
Hôpital Necker-Enfants Malades
Valerie Cormier-Daire
Imagine Institute, Université Paris Cité, INSERM U1163
Sylvain Hanein
Imagine Institute, Université Paris Cité, INSERM U1163
Marine Delvigne
Fondation Elan Retrouvé
Valerie Malan
Hôpital Necker-Enfants Malades
Arnold Munnich
Fondation Elan Retrouvé
Monica Zilbovicius
Ecole Normale Supérieure Paris-Saclay, Université Paris-Saclay, Université Paris Cité, INSERM U1299 “Trajectoires Développementales & Psychiatrie”, Centre Borelli
Nathalie Boddaert
Nathalie.boddaert@aphp.fr

Imagine Institute, Université Paris Cité, INSERM U1163

Research Article

Keywords: Phelan McDermid syndrome, SHANK3, 22q13 deletion syndrome, MRI scan, forceps minor, ADI-R

Posted Date: June 11th, 2026

DOI: https://doi.org/10.21203/rs.3.rs-9779696/v1

License: This work is licensed under a Creative Commons Attribution 4.0 International License. Read Full License

Additional Declarations: No competing interests reported.

Abstract

Background:

Phelan–McDermid syndrome (PMS) is a neurodevelopmental disorder caused by pathogenic variants involving the *SHANK3* gene, a key postsynaptic scaffolding protein regulating synaptic function. *SHANK3* alterations range from sequence variants to large chromosomal deletions on chromosome 22q13. While *SHANK3* haploinsufficiency alone produces core PMS features, larger deletions encompassing adjacent genes are associated with more severe motor, speech, and cognitive phenotypes, whereas smaller deletions may lead to distinct neurobehavioral profiles.

Methods:

We conducted a multimodal study integrating molecular genetics and neuropsychological assessment with structural MRI, voxel-based morphometry (VBM) and arterial spin labeling (ASL) perfusion imaging in 36 individuals with *de novo SHANK3*variants, including 21 sequence variants and 15 deletions ranging from (68.64 kb to 8.7 Mb). Deletions were stratified into Class I (involving *SHANK3* only or with *ARSA*, *ACR*, and/or *RABL2B*) and Class II (all other deletions).

Results:

Class II deletions were strongly associated with cortico-subcortical atrophy (10/15 vs. 0/21; p = 0.00001) and corpus callosum abnormalities. The group with larger deletions (Class II) showed a distinctive anomaly of the forceps minor, characterized by marked enlargement and dysmorphism (8/8 vs 0 in other groups; p < 0.001) and severe nonverbal social communication deficits. This feature was absent in Class I deletions and sequence variants. A minimal 760 kb critical region, including *CERK*, *TBC1D22A*, *CELSR1*, and *GRAMD4*, was implicated in these anomalies. VBM analyses revealed widespread reductions in gray and white matter volumes in carriers of Class II deletions, predominantly in frontotemporal and parietal regions, whereas sequence variants showed no significant volume loss. ASL imaging demonstrated reduced cerebral blood flow in key regions of the social brain network, particularly within the bilateral superior temporal cortex.

Limitations:

Multimodal MRI without premedication remains challenging in children older than 5 years due to motion, particularly with longer acquisition times.

Conclusions:

The identification of a minimal overlapping deleted region encompassing multiple candidate genes supports the contribution of additional loci within 22q13 to disease expression. These findings refine genotype–phenotype correlations in PMS and provide evidence that the disorder associated with larger deletions may be regarded as a contiguous gene syndrome.

Background

Autism spectrum disorder (ASD) is a lifelong neurodevelopmental condition characterized by difficulties in social communication and interaction, alongside restricted and repetitive patterns of behavior and interests [1].Genetic factors are known to play a substantial role, with pathogenic mutations being identified in approximately 30% of individuals with ASD, underscoring the importance of exploring genetic contributions to this condition [2].

Among the ASD genes, *SHANK3* has received considerable attention due to its critical role in synaptic organization and function. The *SHANK3* gene encodes a scaffolding protein located at the postsynaptic density of excitatory synapses where it regulates synaptic signaling, morphology and plasticity. This gene accounts for an estimated 1–2% of ASD cases [3] associated with Phelan–McDermid Syndrome (PMS, OMIM 606232). Disruptions in *SHANK3* lead to synaptic dysfunction and altered neuronal communication, which are thought to underlie complex neurodevelopmental-related phenotypes [4, 5].

A wide spectrum of *SHANK3* alterations has been described, including pathogenic sequence variants, deletions, inversions, and translocations [6–8]. While *SHANK3* haploinsufficiency due to pathogenic sequence variants is sufficient to produce core PMS features, large-scale deletions encompassing additional genes on the 22q13 region often result in more severe motor, speech and cognitive deficits, hypotonia, seizures, and brain abnormalities, often accompanied by psychiatric comorbidities [6, 9–11]. They are also more likely to have psychiatric diagnoses such as bipolar disorder, catatonia, depression, psychotic disorders, and regression [12, 13].

Clinical severity correlates with deletion size, with larger deletions linked to more pronounced features, distinct neurobehavioral profiles and additional comorbidities, including renal anomalies and lymphedema [14, 15].

By integrating molecular genetics, neuropsychological assessment, and multimodal neuroimaging, the present study systematically investigated structural MRI alterations associated with pathogenic *SHANK3* variants across distinct genetic mechanisms and assessed the contribution of arterial spin labeling (ASL) perfusion MRI to the characterization of the underlying pathophysiological processes shared by *SHANK3*-related neurodevelopmental disorders.

Methods

Participants

A total of 36 patients ascertained at Necker University Hospital with pathogenic variants involving the SHANK3 locus between 2015 and 2025 were included in the study (age = 6.02 ± 4.92 y, range = 1-22 y, 16 females and 20 males). All individuals underwent routine clinical investigations including molecular

genetics and brain MRI imaging. Twenty-four patients completed the Autism Diagnostic Interview-Revised (ADI-R), a semi-structured interview conducted with a parent or caregiver, designed to obtain a detailed developmental history related to autism symptoms [16].

This study, combining retrospectively collected and anonymized clinical MRI and ADI-R data was conducted according to the French regulation for which no Institutional Review Board approval is required. The last four patients were included in the context of a prospective amendment approved by a French ethical committee (Committee for the Protection of Persons Est III - 24.00501.000307, 2023-A02668-37) with written informed consent obtained from all parents or legal guardians.

Molecular characterization of disease-causing variants

Pathogenic *SHANK3* variants were identified by comparative genomic hybridization array, targeted panel sequencing or whole-exome sequencing (WES). All variants were annotated in accordance with the Human Genome Variation Society (HGVS) guidelines. The results refer to the *SHANK3* RefSeq mRNA (NM_001372044.2) and protein sequences (NP_001358973.1). The in silico functional consequences of the variants were assessed using Alamut Visual software (version 2.14), integrating predictive algorithms such as SIFT and PolyPhen-2, along with curated pathogenicity databases. In addition, the UCSC Genome Browser was used to visualize the genomic context of each variant, including neighboring genes and regulatory regions. The deletions were classified in two categories according to their size as described by Levy et al. (6). Class I deletions include only *SHANK3* or *SHANK3* in combination with *ARSA* and/or *ACR* and *RABL2B*. Class II deletions include all deletions that did not qualify as Class I as described

Brain MRI

Brain MRI 3DT1, T2 and FLAIR sequences were available for all patients. Scans were obtained on either a 1.5T MRI scanner (n=24) or a 3T MRI scanner (n=12) from General Electric Healthcare at the Pediatric Radiology Department of Necker Hospital in Paris, France. Sedation (rectal pentobarbital, 5 mg/kg) was administered to children below 25 kg according to standard protocol. No sedation was applied to patients above 25 kg. ASL MRI sequence was acquired in a subgroup of 7 patients.

All anatomical images (T1, T2, FLAIR) were examined by two seniors pediatric neuroradiologists (NB, SC) not aware of individual genetic status. To ensure greater objectivity, biometric measurements were subsequently performed, focusing on the morphological anomalies identified on image reviews, notably involving the forceps minor. The forceps minor, also known as the anterior forceps, is a white matter fiber bundle connecting the lateral and medial surfaces of the frontal lobes and crossing the midline through the genu of the corpus callosum. For quantitative assessment, the forceps minor was measured on the axial T1-weighted slice passing through the insula. We compared MRI scanner of patients carrying pathogenic variants involving the *SHANK3* locus with 50 controls matched for age (mean age 7.85-±7 y, 17 females and 33 males). Control subjects were selected from the Radiology department database and did not suffer from central nervous system conditions (arthrogryposis, lymphangioma, morphological evaluation of upper-limit head circumference, subcutaneous cyst, benign nystagmus, isolated strabismus and neonatal diabetes). Routine clinical brain MRI were performed.

When feasible, an ASL sequence was also performed on the same 3T MRI scanner. ASL perfusion images were performed with a 3D pseudo continuous arterial spin labelling (3D pcASL) sequence using a fast spin echo acquisition with spiral spilling of the k-space (TR = 4453 ms; TE = 10.96 ms; 8 spiral alarms x 512 sampling points; Freq = 512 ; post labelling delay (PLD) = 1025 ms; labelling duration = 1500 ms; FA = 155°; matrix size = 128x128 ; resolution in plane = 1.875x1.875 mm; slice thickness = 4 mm; field of view = 24x24 cm; bandwidth = 62.50 ; imaging options EDR, Fast Spiral, Phase8 Freq, NEX 3.00, Auto Shim On, 40 contiguous axial slices and duration time = 4 min).

Voxel based morphometry (VBM) group comparison

To investigate cortical grey matter (GM) and white matter (WM), 3D T1-weighted images were processed using SPM12 and CAT12, including normalization to MNI space, segmentation into GM/WM/cerebrospinal fluid, and bias correction. GM maps were modulated and smoothed (10 mm FWHM). Subjects with failed preprocessing due to motion or artefacts were excluded.

To investigate cortical grey matter (GM) and white matter (WM), a whole-brain voxel-wise analysis was performed within the framework of the GLM in SPM12 comparing patients to age-matched controls. In addition, we performed the same analyses comparing patients classified in Class I and patients with sequence variants compared to age-matched controls and patients classified in Class II compared to age-matched controls. Age and scanners were considered as covariates in all statistical models. Analyses were performed on the smoothed, normalized images. The significance threshold was set at $p < 0.05$ FWE correction for multiple comparisons.

Arterial Spin labelling (ASL) group comparison of relative cerebral blood flow at rest

ASL images were visually inspected, co-registered to native GM, normalized to MNI space, and smoothed (6 mm FWHM) using SPM12. Subjects with failed preprocessing due to motion or artefacts were excluded. To compare relative cerebral blood flow (rCBF) at rest, obtained from ASL images, we performed a whole-brain voxel-wise analysis within the framework of the general linear model (GLM) in SPM12 and compared patients to age-matched controls. Age was considered as covariate in the statistical model. Statistical thresholds were set at the cluster-level at $p < 0.05$ corrected for multiple comparisons using family-wise error (FWE) correction and a cluster threshold of 50 voxels was applied. Age-matched control subjects for VBM and ASL were selected among the 50 controls from the Radiology department database as mentioned above. Fisher's exact test was used to assess statistical differences between groups. We performed a t-test to compare age variables and Fisher's test to compare sex variables after checking the normality distribution of the variables using Shapiro-Wilk test.

Results

Genetic findings

All pathogenic variants occurred de novo (details for all patients are described in Table 1 and Fig.1). *SHANK3* sequence variants represented the majority of cases (21/36 patients, 58.5%) while deletions encompassing the *SHANK3* gene were observed in the remaining 41.5% (15/36 patients), with deletion sizes ranging from 68.64 kb to 8.702 Mb (mean size: 4.44 Mb). The deletions were classified in two categories according to their size as described by Levy et al. Class I deletions include only *SHANK3* or *SHANK3* in combination with *ARSA* and/or *ACR* and *RABL2B*. The latter three genes are unlikely to influence the PMS phenotype, as they do not exhibit intolerance to protein-truncating variants (pLI = 0 in the gnomAD database). Furthermore, *ARSA* is associated with metachromatic leukodystrophy, an autosomal recessive condition. Class II include all deletions that did not qualify as Class I as described. For most genotype–phenotype analyses, Class I deletions and sequence variants were grouped together. The Class I deletion and sequence variant group included 22 patients (one with Class I deletion and 21 with sequence variants), while the Class II deletion group comprised 14 participants.

MRI findings

Blind examination of brain MRIs revealed that none of the *SHANK3* sequence variants (patients 16-36, Table 1), but the majority of deletions spanning genes proximal to *SHANK3* on chromosome 22q, were associated with cortical/subcortical atrophy (deletions 10/15 vs variants 0/21; $p = 0.00001$) and/or with thin, dysmorphic corpus callosum (deletions 11/15 cases, 73% vs variants 0/21; $p < 0.0001$). Notably, no epilepsy was reported in patients with cortical atrophy. These anomalies were associated with Class II deletions (see Figure 1) but not with Class I deletions or *SHANK3* sequence variants. Similarly, no Class I deletions or *SHANK3* variants but several large Class II deletions spanning 6-8.7 Mb were associated with septal cysts, cerebellar dysplasia, ectopic posterior pituitary, midline malformations or abnormal temporal lobe myelination (Table 1).

Interestingly, the forceps minor was consistently abnormal in Class II patients carrying large-scale deletions ranging in size from 6 Mb to 8.7 Mb, but in none of the patients carrying smaller Class II deletions ranging from 486 kb to 4.37 Mb, intragenic deletions or *SHANK3* sequence variants. The forceps minor normally appears as a small, round, non-elongated structure with a mean thickness of 3.3 mm. It is clearly visible in control children under one year and it remains consistently small later, measuring <6 mm before one year and <5 mm thereafter. In PMS, diffusion MRI tractography showed a markedly reduced number of white matter fibers in the corpus callosum and distinctive forceps minor anomalies in patients carrying large-scale Class II deletions (Fig.3, patients 8–15; 8/8, Table 1). Their forceps minor was abnormally long, elongated, and significantly larger in size (>7 mm) compared with 50 age-matched controls (<5 mm; $p < 0.001$) (Fig. 2). It remained visible on both T1 and T2-weighted images and appeared hypointense on T1-weighted images and hyperintense on T2-weighted and FLAIR sequences. Conversely, in patients carrying *SHANK3* sequence variants, the MRI appearance of the forceps minor was similar to that of age-matched controls with respect to size, thickness and morphology. Likewise, none of the patients carrying smaller, more distal deletions ranging from 486 kb to 4.37 Mb exhibited an abnormal forceps minor (mean thickness 3.3 mm). Group comparisons showed significant differences between large-scale Class II deletions (6 Mb to 8.7 Mb) with abnormal forceps minor vs smaller Class II deletions (486 kb to 4.37 Mb) ($t = 4.302$; $p = 0.0012$) and vs Class I and *SHANK3* sequence variants ($t = 5.99$; $p < 0.001$).

Figure 1 shows that the minimal chromosomal interval associated with forceps minor anomalies encompassed 760.284 kb (GRCh38/hg38) and spanned at least four genes, namely *CERK, TBC1D22A, CELSR1*, and *GRAMD4*. The probability of loss-of-function intolerance (pLI) is 0 for *CERK, CELSR1, and TBC1D22A* (Genome Aggregation Database, gnomAD v4.1.1)[17] whereas *GRAMD4* has a pLI of 1, consistent with a high sensitivity to haploinsufficiency.

In order to further document our brain MRI findings in PMS, we performed whole-brain voxel-based morphometry (VBM) analyses to investigate cortical white and grey matter in a subset of participants for whom high-quality 3D T1-weighted images were available. The final sample included 27 patients (15 males; age 4.40 ± 2.55 y) and 39 controls (19 males; age 3.95 ± 2.36 y).

VBM analyses showed that patients carrying pathogenic Class I deletions or *SHANK3* variants exhibited no significant reduction in white and gray matter volume compared to controls ($p < 0.05$, FWE corrected). Conversely, a significant widespread reduction in total white and grey matter volumes was observed in the Class II deletion group (13 patients, 7 males; age 3.09 ± 2.08 y) compared with individuals carrying Class I deletions or *SHANK3* sequence variants (14 patients, 8 males; age 5.61 ± 2.23 y) ($p < 0.05$, FWE corrected). When analyzed separately, patients with Class II deletions showed a significant reduction of frontotemporal and parietal white matter volume and striatal volume compared to controls ($p < 0.05$, FWE corrected), whereas no significant gray or white matter volume differences were observed in Class I deletions or sequence variants relative to controls. No regions showed increased gray or white matter volume in any comparison.

ASL-MRI sequences for assessment of rCBF were available in 7/36 patients carrying either Class I or II deletions or *SHANK3* sequence variants (Class II deletion group: 2/7; Class I deletion: 1/7 or sequence variants: 4/7; 3 males, age 3.40 ± 1.10 y,). ASL data were compared to 21 age-matched controls (age 3.22 ± 0.86 y, range 1-5 y, 10 males). ASL analysis showed a significant decrease of rCBF in all, mainly localized in the bilateral superior temporal regions (clusters 1 to 4), bilateral superior frontal regions (clusters 5 to 8), the left mesial precentral gyrus (cluster 9) and left supramarginal gyrus (cluster 10) ($p < 0.05$, FWE corrected). No increase of whole brain rCBF was found in our series compared to controls (Fig.4).

ADI-R findings

Autism Diagnostic Interview-Revised (ADI-R) scores were obtained for 26 patients (Table 1). Scores were all above cut-off values for social interactions (module A) and differences between genetic classes were not significant (Class II vs Class I deletions and sequence variants: $t = 2.03$ $p = 0.053$). Regarding language and communication (module B, verbal and nonverbal), only the non-verbal communication score (BNV) was applicable, as 23/26 patients were nonverbal. Interestingly, patients with a forceps minor anomaly exhibited significantly higher BNV sub-scores, indicating more severe social communication difficulties. The BNV score gave highly significant differences between genetic classes (large-scale vs small Class II deletions: $t = 5.21$; $p = 0.0003$; large-scale Class II vs Class I deletions and sequence variants: $t = 5.46$; $p < 0.0001$). Finally, scoring of repetitive behaviors and interests/stereotypies (module C),

was compromised by intellectual, language and motor difficulties, hypotonia, and hyposensitivity, and differences between genetic classes were not significant (large-scale vs small Class II deletions: t = 0.47; p = 0.648; Class II vs Class I deletions and sequence variants: t = 1.12; p = 0.27).

Discussion

Using multimodal brain neuroimaging in a cohort of PMS patients stratified in distinct classes of disease mechanisms, we identified several MRI signs in PMS. We found that none of Class I deletions or *SHANK3* sequence variants, but all Class II deletions caused consistent patterns of structural brain abnormalities, including cortico-subcortical atrophy and corpus callosum abnormalities. Our findings suggest that both the severity and degree of MRI abnormalities are influenced by the underlying genetic mechanism and deletion size.

A previous study of patients with 22q13 deletions and epilepsy reported mild cortical atrophy and other nonspecific MRI abnormalities, including ventricular enlargement, delayed myelination, and corpus callosum anomalies [18, 19]. Consistently, nonspecific cortical atrophy has been reported in adolescents and adults with PMS presenting neuropsychiatric regression and decompensation [12]. Earlier studies, including the seminal work by Philippe *et al*. [20], previously highlighted the heterogeneity of neuroimaging findings in 22q13 deletion and the absence of specific radiological signature. Taken together, these results support the view that neuroimaging abnormalities in PMS are frequent but heterogeneous and largely nonspecific, as recently emphasized in the consensus guidelines on PMS management [21].

Our findings are in line with recent genotype–phenotype studies demonstrating that larger 22q13 deletions are associated with increased neurological severity and a higher frequency of neuroimaging abnormalities, including ventricular abnormalities, decreased gray matter volume (atrophy), hypomyelination, and arachnoid cysts [22]. Our voxel-based morphometry analyses further document widespread reduction of gray and white matter volumes in patients carrying Class II deletions, whereas no significant volumetric abnormalities were identified in patients with *SHANK3* sequence variants or Class I deletions. Our voxel-based morphometry also shows that patients carrying Class II deletions exhibited significant widespread frontal, parietal and temporal white matter volume reduction, together with decreased striatal gray matter volume. Moreover, MRI diffusion tractography showed a marked reduction in the number of white matter fibers in the forceps minor and the corpus callosum region, supporting the concept of a more diffuse neurodevelopmental involvement associated with Class II deletions. Hence, our findings further support conventional MRI observations of more severe and widespread neuroanatomical involvement associated with Class II deletions. Along those lines, previous studies have reported structural alterations of the striatum, the caudate nuclei, the putamen, and to a lesser extent, the globus pallidus together with cerebellar abnormalities of the cerebellar vermis and the frontotemporal region implicated in social cognition in individuals with PMS [23, 24].

Importantly, most large-scale Class II deletions (6 to 8.7 Mb, 8 patients) but none of Class I deletions or sequence variants or smaller Class II deletions (486 kb to 4.37 Mb) were associated with an abnormal forceps minor. The forceps minor is an interhemispheric white matter fiber tract forming the genu of the corpus callosum and connecting the orbitofrontal cortices [25], and has been implicated in social behavior networks [26]. Interestingly, patients with a forceps minor anomaly exhibited significantly higher B-nonverbal (BNV) sub-score, which may reflect greater overall impairment, including social communication difficulties. Even though this association should be interpreted with caution, as it could reflect the overall severity of neurodevelopmental impairment associated with larger deletions rather than a specific structure–function relationship, it is consistent with established genotype–phenotype correlations in PMS, showing that larger deletions encompassing additional genes are associated with more severe clinical phenotypes and brain imaging abnormalities.

Importantly, we report here what we believe to be the first ASL-MRI evidence of bilateral superior temporal sulcus (STS) hypoperfusion in PMS. STS is a key component of the social brain network [27] and plays a major role in biological motion perception, gaze processing, and theory of mind [28, 29]. Hypoperfusion within this region is consistent with previous functional MRI studies reporting altered connectivity of temporal and frontal networks in ASD as well as in *SHANK3*-deficient animal models. In particular, *SHANK3*-mutant macaques exhibit social withdrawal, repetitive behaviors, and disrupted resting-state connectivity involving temporal, frontal, and sensorimotor regions [30]. Our findings further support the concept that PMS is associated with functional network abnormalities affecting brain circuitry involved in social cognition.

Interestingly, previous diffusion tensor imaging (DTI) studies have suggested that PMS is associated with abnormalities of structural connectivity, including alterations of frontotemporal associative pathways such as the uncinate fasciculus and inferior longitudinal fasciculus [31]. More recently, Jesse et al. [32] reported diffuse microstructural white matter abnormalities involving the corpus callosum, dorsal cingulum, and corticospinal tracts. These findings are consistent with the frontal white matter alterations identified in our cohort and support the concept of impaired associative and commissural white matter pathways in PMS, particularly in individuals carrying large Class II deletions.

Finally, we delineated the smallest region of overlap (760.284 kb) that likely contributes to the severity of large-scale 22q13.2–q13.33 deletions, with respect to non-verbal communication, scarcity of white matter fibers and anomalies of the forceps minor. Although *SHANK3* haploinsufficiency is considered the principal driver of the neurodevelopmental phenotype, loss of additional genes within the 22q13 deleted interval is thought to underlie several systemic manifestations. The question of whether one single gene or a combination of genes involved in large-scale Class II deletions causes disruption of the structural integrity of the forceps minor and impaired nonverbal social behavior has not yet been answered. Similarly, whether forceps minor anomalies are the direct consequence of haploinsufficiency of any of these genes or reflect white matter fiber loss and network disorganization remains unclear.

At least four genes are located within the smallest region of overlap: *CERK, TBC1D22A, CELSR1*, and *GRAMD4*. *CERK* encodes ceramide kinase, which catalyzes the formation of ceramide-1-phosphate, a bioactive lipid involved in membrane dynamics, inflammatory signaling, and cell survival pathways [33]. Although its biochemical function is well established, there is currently no conclusive evidence linking *CERK* to a defined monogenic human disorder. *TBC1D22A* encodes a TBC domain–containing protein that likely functions as a Rab GTPase-activating protein involved in intracellular vesicular trafficking

[34]. Although vesicle trafficking pathways are important for neuronal function, there is no direct evidence linking TBC1D22A variants to a specific human disorder.

CELSR1 encodes a protocadherin essential for planar cell polarity signaling during embryogenesis [35]. Beyond its established developmental and cellular functions, *CELSR1* may also contribute to the clinical variability observed in PMS. *CELSR1*, encompassed by terminal deletions larger than 4.3 Mb, is a strong candidate gene given its established association with autosomal dominant primary lymphedema [36, 37]. Indeed, lymphedema has been reported in PMS individuals carrying larger terminal deletions (> 4.3 Mb) [6, 15, 22], supporting *CELSR1* dosage sensitivity in the disease.

On the other hand, *GRAMD4* encodes a p53-inducible protein implicated in mitochondrial apoptosis. Despite its defined molecular function, current evidence linking *GRAMD4* to human disease remains limited [38]. Yet, based on the pLI predictive metric and the LOEUF score of 0.416, haploinsufficiency of *GRAMD4* may be also regarded as possibly responsible for severity of the phenotype associated with large deletions.

To date, only two autosomal dominant genes located in the interval deleted in PMS are referenced in the Mendelian Inheritance in Man (OMIM®) catalog of human disease genes, namely *TCF20* and *CELSR1*. *TCF20* is located more proximally in the 22q13.2 region and is not included within the smallest region of overlap identified in our cohort (760.284 kb). However, it has been implicated in individuals with larger terminal deletions (> 8.6 Mb), where haploinsufficiency leads to a distinct neurodevelopmental syndrome characterized by motor and language delay, intellectual disability, ASD, hypotonia, and variable dysmorphic features [39, 40]. This suggests that *TCF20* contributes to the broader phenotypic spectrum observed in extended 22q13 deletions rather than the core SRO-related phenotype.

In addition, the delineation of a minimal overlapping region reported here further supports the view that 22q13 deletion-related disorders should be regarded as a contiguous gene syndrome, with combined effects on brain structure, white matter organization, and neurodevelopmental outcome.

Limitations

This study has several limitations. First, the retrospective inclusion of part of the cohort who underwent routine clinical MRI, precluded the use of advanced sequences such as multi-directional DTI and resting-state imaging in all. Future prospective studies will include these modalities alongside ASL. Second, ASL analyses were limited by the small number of motion-free datasets acquired on a single 3T scanner, as inclusion of data from different MRI systems would have introduced variability and reduced data consistency. They were restricted to premedicated children (under 5 years old) to ensure homogeneity. Despite prospective acquisition of DTI, resting-state, and ASL sequences, too few non-premedicated children yielded usable data. Multimodal MRI without premedication remains challenging in children older than 5 years due to motion, particularly with longer acquisition times.

Finally, the lack of functional genomic analyses also restricts our ability to directly correlate pathogenic variants to protein dysfunction. Further research will use the Vineland scale to better assess the level of adaptive development and decide whether the communication deficit is a primary issue or the consequence of a more severe level of functional disability. Future studies aimed at replicating these observations in larger, multicentric cohorts will also further refine genotype-phenotype correlations in what we believe to be a novel contiguous gene syndrome.

Conclusions

This study adds new insights to the underpinnings of *SHANK3*-related neurodevelopmental disorders through multimodal neuroimaging. Our findings reveal distinctive structural and functional brain alterations in PMS and show that the severity and distribution of radiological abnormalities are modulated by the underlying genetic mechanisms, particularly in the context of Class II deletions. The identification of forceps minor anomalies and superior temporal sulcus hypoperfusion further supports the involvement of disturbed brain networks underlying social cognition deficits. These results emphasize the value of integrating genetic information to the interpretation of neuroimaging findings. Future studies combining advanced imaging and functional genomics will hopefully elucidate the mechanisms linking genetic variation to brain dysfunction in this condition.

Abbreviations

ADI-R: Autism Diagnostic Interview-Revised

ASD: Autism spectrum disorder

ASL: Arterial spin labeling

BNV: Non-verbal communication score (ADI-R subdomain)

CBF: Cerebral blood flow

DTI: Diffusion tensor imaging

FWE: Family-wise error

GLM: General linear model

gnomAD: Genome Aggregation Database

HGVS: Human Genome Variation Society

LOEUF: Loss-of-function observed/expected upper bound fraction

MNI: Montreal Neurological Institute

MRI: Magnetic resonance imaging

mRNA: Messenger ribonucleic acid

OMIM: Online Mendelian Inheritance in Man

pLI : Probability of loss-of-function intolerance

PMS: Phelan–McDermid syndrome

RefSeq: Reference sequence

SPM12: Statistical Parametric Mapping (version 12)

STS: Superior temporal sulcus

VBM: Voxel-based morphometry

WES: Whole-exome sequencing

Declarations

Ethics approval and consent to participate

Ethics approval and consent to participate: This study, combining retrospectively collected and anonymized clinical MRI and ADI-R data was conducted according to the French regulation for which no Institutional Review Board approval is required. The last four patients were included in the context of a prospective amendment approved by a French ethical committee (Committee for the Protection of Persons Est III - 24.00501.000307, 2023-A02668-37) with written informed consent obtained from all parents or legal guardians.

Consent for publication:

Not applicable

Availability of data and materials

All data supporting the findings of this study are available upon request.

Competing interests

The authors declare that they have no competing interests.

Funding

This retrospective study is based on routine medical care of patients at Necker University Hospital.

Authors' contributions

KA contributed to data acquisition, data analysis, and writing of the main manuscript. AF performed all autism diagnostic interviews. JB, SC and LF participated in data analyses. AP contributed to data acquisition and revision of the manuscript. AS, SH prepared figures and contributed to revision of the manuscript. MR and VM contributed to recruitment. MD contributed to data analysis. VC-D and VD-R contributed to revision of the manuscript. AM, NB and MZ contributed to data acquisition, study design, revision of paper and supervising the work. All authors read and approved the final manuscript.

References

1. Rosen NE, Lord C, Volkmar FR. The Diagnosis of Autism: From Kanner to DSM-III to DSM-5 and Beyond. J Autism Dev Disord. 2021;51:4253–70. https://doi.org/10.1007/s10803-021-04904-1.
2. Munnich A, Demily C, Frugère L, Duwime C, Malan V, Barcia G, et al. Impact of on-site clinical genetics consultations on diagnostic rate in children and young adults with autism spectrum disorder. Mol Autism. 2019;10:33. https://doi.org/10.1186/s13229-019-0284-2.
3. Sarasua SM, Dwivedi A, Boccuto L, Chen C-F, Sharp JL, Rollins JD, et al. 22q13.2q13.32 genomic regions associated with severity of speech delay, developmental delay, and physical features in Phelan-McDermid syndrome. Genet Med. 2014;16:318–28. https://doi.org/10.1038/gim.2013.144.
4. Frank Y. The Neurological Manifestations of Phelan-McDermid Syndrome. Pediatr Neurol. 2021;122:59–64. https://doi.org/10.1016/j.pediatrneurol.2021.06.002.

5. De Rubeis S, Siper PM, Durkin A, Weissman J, Muratet F, Halpern D, et al. Delineation of the genetic and clinical spectrum of Phelan-McDermid syndrome caused by SHANK3 point mutations. Mol Autism. 2018;9:31. https://doi.org/10.1186/s13229-018-0205-9.
6. Levy T, Foss-Feig JH, Betancur C, Siper PM, Trelles-Thorne MDP, Halpern D, et al. Strong evidence for genotype-phenotype correlations in Phelan-McDermid syndrome: results from the developmental synaptopathies consortium. Hum Mol Genet. 2022;31:625–37. https://doi.org/10.1093/hmg/ddab280.
7. Doheny KF, McDermid HE, Harum K, Thomas GH, Raymond GV. Cryptic terminal rearrangement of chromosome 22q13.32 detected by FISH in two unrelated patients. J Med Genet. 1997;34:640–4. https://doi.org/10.1136/jmg.34.8.640.
8. Disciglio V, Lo Rizzo C, Mencarelli MA, Mucciolo M, Marozza A, Di Marco C, et al. Interstitial 22q13 deletions not involving SHANK3 gene: a new contiguous gene syndrome. Am J Med Genet A. 2014;164A:1666–76. https://doi.org/10.1002/ajmg.a.36513.
9. Leblond CS, Nava C, Polge A, Gauthier J, Huguet G, Lumbroso S, et al. Meta-analysis of SHANK Mutations in Autism Spectrum Disorders: A Gradient of Severity in Cognitive Impairments. PLoS Genet. 2014;10:e1004580. https://doi.org/10.1371/journal.pgen.1004580.
10. Nevado J, García-Miñaúr S, Palomares-Bralo M, Vallespín E, Guillén-Navarro E, Rosell J, et al. Variability in Phelan-McDermid Syndrome in a Cohort of 210 Individuals. Front Genet. 2022;13:652454. https://doi.org/10.3389/fgene.2022.652454.
11. Durand CM, Betancur C, Boeckers TM, Bockmann J, Chaste P, Fauchereau F, et al. Mutations in the gene encoding the synaptic scaffolding protein SHANK3 are associated with autism spectrum disorders. Nat Genet. 2007;39:25–7. https://doi.org/10.1038/ng1933.
12. Kolevzon A, Delaby E, Berry-Kravis E, Buxbaum JD, Betancur C. Neuropsychiatric decompensation in adolescents and adults with Phelan-McDermid syndrome: a systematic review of the literature. Mol Autism. 2019;10:50. https://doi.org/10.1186/s13229-019-0291-3.
13. Kohlenberg TM, Trelles MP, McLarney B, Betancur C, Thurm A, Kolevzon A. Psychiatric illness and regression in individuals with Phelan-McDermid syndrome. J Neurodev Disord. 2020;12:7. https://doi.org/10.1186/s11689-020-9309-6.
14. Sarasua SM, Dwivedi A, Boccuto L, Rollins JD, Chen C-F, Rogers RC, et al. Association between deletion size and important phenotypes expands the genomic region of interest in Phelan-McDermid syndrome (22q13 deletion syndrome). J Med Genet. 2011;48:761–6. https://doi.org/10.1136/jmedgenet-2011-100225.
15. Samogy-Costa CI, Varella-Branco E, Monfardini F, Ferraz H, Fock RA, Barbosa RHA, et al. A Brazilian cohort of individuals with Phelan-McDermid syndrome: genotype-phenotype correlation and identification of an atypical case. J Neurodev Disord. 2019;11:13. https://doi.org/10.1186/s11689-019-9273-1.
16. Lord C, Rutter M, Le Couteur A. Autism Diagnostic Interview-Revised: a revised version of a diagnostic interview for caregivers of individuals with possible pervasive developmental disorders. J Autism Dev Disord. 1994;24:659–85. https://doi.org/10.1007/BF02172145.
17. Gudmundsson S, Singer-Berk M, Watts NA, Phu W, Goodrich JK, Solomonson M, et al. Variant interpretation using population databases: Lessons from gnomAD. Hum Mutat. 2022;43:1012–30. https://doi.org/10.1002/humu.24309.
18. Figura MG, Coppola A, Bottitta M, Calabrese G, Grillo L, Luciano D, et al. Seizures and EEG pattern in the 22q13.3 deletion syndrome: clinical report of six Italian cases. Seizure. 2014;23:774–9. https://doi.org/10.1016/j.seizure.2014.06.008.
19. Holder JL, Quach MM. The spectrum of epilepsy and electroencephalographic abnormalities due to SHANK3 loss of function mutations. Epilepsia. 2016;57:1651–9. https://doi.org/10.1111/epi.13506.
20. Philippe A, Boddaert N, Vaivre-Douret L, Robel L, Danon-Boileau L, Malan V, et al. Neurobehavioral profile and brain imaging study of the 22q13.3 deletion syndrome in childhood. Pediatrics. 2008;122:e376–382. https://doi.org/10.1542/peds.2007-2584.
21. Srivastava S, Sahin M, Buxbaum JD, Berry-Kravis E, Soorya LV, Thurm A, et al. Updated consensus guidelines on the management of Phelan-McDermid syndrome. Am J Med Genet A. 2023;191:2015–44. https://doi.org/10.1002/ajmg.a.63312.
22. Yin R, Wack M, Hassen-Khodja C, McDuffie MT, Bliss G, Horn EJ, et al. Phenome-wide profiling identifies genotype-phenotype associations in Phelan-McDermid syndrome using family-sourced data from an international registry. Mol Autism. 2024;15:40. https://doi.org/10.1186/s13229-024-00619-z.
23. Srivastava S, Scherrer B, Prohl AK, Filip-Dhima R, Kapur K, Kolevzon A, et al. Volumetric Analysis of the Basal Ganglia and Cerebellar Structures in Patients with Phelan-McDermid Syndrome. Pediatr Neurol. 2019;90:37–43. https://doi.org/10.1016/j.pediatrneurol.2018.09.008.
24. Liu C, Li D, Yang H, Li H, Xu Q, Zhou B, et al. Altered striatum centered brain structures in SHANK3 deficient Chinese children with genotype and phenotype profiling. Prog Neurobiol. 2021;200:101985. https://doi.org/10.1016/j.pneurobio.2020.101985.
25. Goldstein A, Covington BP, Mahabadi N, Mesfin FB, Neuroanatomy. Corpus Callosum. StatPearls [Internet]. Treasure Island (FL): StatPearls Publishing; 2026 [cited 2026 Apr 10]. http://www.ncbi.nlm.nih.gov/books/NBK448209/. Accessed 10 Apr 2026.
26. Stoller F, Hinds E, Ionescu T, Khatamsaz E, Marston HM, Hengerer B. Forceps minor control of social behaviour. Sci Rep. 2024;14:30492. https://doi.org/10.1038/s41598-024-81930-w.
27. Saitovitch A, Bargiacchi A, Chabane N, Brunelle F, Samson Y, Boddaert N, et al. Social cognition and the superior temporal sulcus: implications in autism. Rev Neurol (Paris). 2012;168:762–70. https://doi.org/10.1016/j.neurol.2012.07.017.
28. Deen B, Koldewyn K, Kanwisher N, Saxe R. Functional Organization of Social Perception and Cognition in the Superior Temporal Sulcus. Cereb Cortex. New York, N.Y.: 1991; 2015;25:4596–609. https://doi.org/10.1093/cercor/bhv111
29. Lahnakoski JM, Glerean E, Salmi J, Jääskeläinen IP, Sams M, Hari R, et al. Naturalistic fMRI Mapping Reveals Superior Temporal Sulcus as the Hub for the Distributed Brain Network for Social Perception. Front Hum Neurosci [Internet] Front. 2012. https://doi.org/10.3389/fnhum.2012.00233. [cited 2026 Apr 10];6.
30. Zhou Y, Sharma J, Ke Q, Landman R, Yuan J, Chen H, et al. Atypical behaviour and connectivity in SHANK3-mutant macaques. Nature. 2019;570:326–31. https://doi.org/10.1038/s41586-019-1278-0.

31. Bassell J, Srivastava S, Prohl AK, Scherrer B, Kapur K, Filip-Dhima R, et al. Diffusion Tensor Imaging Abnormalities in the Uncinate Fasciculus and Inferior Longitudinal Fasciculus in Phelan-McDermid Syndrome. Pediatr Neurol. 2020;106:24–31. https://doi.org/10.1016/j.pediatrneurol.2020.01.006.
32. Jesse S, Müller H-P, Huppertz H-J, Andres S, Ludolph AC, Schön M, et al. Neurodegeneration or dysfunction in Phelan-McDermid syndrome? A multimodal approach with CSF and computational MRI. Orphanet J Rare Dis. 2023;18:274. https://doi.org/10.1186/s13023-023-02863-7.
33. Cerk IK, Wechselberger L, Oberer M. Adipose Triglyceride Lipase Regulation: An Overview. Curr Protein Pept Sci. 2018;19:221–33. https://doi.org/10.2174/1389203718666170918160110.
34. Fukuda M. Regulation of secretory vesicle traffic by Rab small GTPases. Cell Mol Life Sci. 2008;65:2801–13. https://doi.org/10.1007/s00018-008-8351-4.
35. Robinson A, Escuin S, Doudney K, Vekemans M, Stevenson RE, Greene NDE, et al. Mutations in the planar cell polarity genes CELSR1 and SCRIB are associated with the severe neural tube defect craniorachischisis. Hum Mutat. 2012;33:440–7. https://doi.org/10.1002/humu.21662.
36. Gonzalez-Garay ML, Aldrich MB, Rasmussen JC, Guilliod R, Lapinski PE, King PD, et al. A novel mutation in CELSR1 is associated with hereditary lymphedema. Vasc Cell. 2016;8:1. https://doi.org/10.1186/s13221-016-0035-5.
37. Maltese PE, Michelini S, Ricci M, Maitz S, Fiorentino A, Serrani R, et al. Increasing evidence of hereditary lymphedema caused by CELSR1 loss-of-function variants. Am J Med Genet A. 2019;179:1718–24. https://doi.org/10.1002/ajmg.a.61269.
38. John K, Alla V, Meier C, Pützer BM. GRAMD4 mimics p53 and mediates the apoptotic function of p73 at mitochondria. Cell Death Differ. 2011;18:874–86. https://doi.org/10.1038/cdd.2010.153.
39. Torti E, Keren B, Palmer EE, Zhu Z, Afenjar A, Anderson IJ, et al. Variants in TCF20 in neurodevelopmental disability: description of 27 new patients and review of literature. Genet Med. 2019;21:2036–42. https://doi.org/10.1038/s41436-019-0454-9.
40. Vetrini F, McKee S, Rosenfeld JA, Suri M, Lewis AM, Nugent KM, et al. De novo and inherited TCF20 pathogenic variants are associated with intellectual disability, dysmorphic features, hypotonia, and neurological impairments with similarities to Smith-Magenis syndrome. Genome Med. 2019;11:12. https://doi.org/10.1186/s13073-019-0623-0.
41. The Human Central Nervous System. AJNR Am J Neuroradiol. 2008;29:e39. https://doi.org/10.3174/ajnr.A0991. 4th ed..

Tables

Table 1. Forceps minor morphology, radiological abnormalities and ADI-R scores in Phelan–McDermid syndrome patients with Class I deletions, Class II deletions and *SHANK3* sequence variants

Patients	*Genetic class*	*Deletion size and sequence variants*	*Age (y)*	*Forceps minor size (N<5mm)*	*Forceps minor shape*	*ADI – A (cut off ≥ 10)*	*ADI - BNV (cut off ≥ 7)*	*ADI - C (cut off ≥ 3)*	*Radiological abnormalities*			
									Cortical atrophy	**Dysmorphic corpus callosum**	**Septal cyst**	**Cerebellar dysplasia**
	Class II deletions (D: ≥ 4 Mb, GRCh38)											
P1	g.42080018_50739836del	8.7 Mb	3.6	5.5	Linear	27	21	21	+	+	+	+
P2	g.42610200_50755252del	8.1 Mb	2.6	5.2	Linear	26	20	15	_	_	_	_
P3	g.42869699_50739896del	7.9 Mb	1.2	7.2	Linear	37	21	14	+	+	_	_
P4	g.44374846_50755252del	6.8 Mb	1.9	5.9	Linear	16	19	5	+	+	+	_
P5	g.44374846_50739836del	6.4 Mb	7.7	10.9	Linear	ND	ND	ND	+	+	+	_
P6	g.44746947_50739836del	6.4 Mb	1.1	9.3	Linear	23	20	10	+	+	_	_
P7	g.47174002_50739836del	6 Mb	1.9	7.3	Linear	31	21	14	+	+	_	+
P8	g.48143023_50739836del	4.3 Mb	1.2	7.4	Linear	41	21	21	_	_	_	_
	Class II deletion (d: < 4 Mb, GRCh38)											
P9	g.47174002_50739836del	3.6 Mb	0.9	2.1	Round	20	16	18	+	+	_	_
P10	g.48143023_50739836del	2.6 Mb	2.6	2.8	Round	25	8	7	+	+	_	_
P11	g.48406294_50780581del	2.4 Mb	7.1	2	Round	27	14	9	+	+	_	_
P12	g.49779271_50739836del	961 kb	3.9	4.7	Round	30	15	24	+	+	_	_
P13	g.49862097_50739836del	878 kb	1.4	5	Linear	27	12	10	_	+	_	_
P14	g.50253782_50739836del	486 kb	3.4	3.7	Linear	28	16	6	_	_	_	_
	Class I deletions & sequence variants											
P15	g.50666119_50734764del	69 kb	3.5	2	Round	21	14	10	_	_	_	_
P16	c.2490+1G>A; p.?	1 bp	4.5	4.9	Linear	26	13	11	_	_	_	_
P17	c.2575+1G>A; p.?	1 bp	6.9	4.7	Linear	21	5	8	_	_	_	_
P18	c.2838C>A; p.(Tyr946Ter)	1 bp	8.8	2.5	Round	ND	ND	ND	_	_	_	_
P19	c.3194_3197delinsCC; p.(Arg1065ProfsTer305)	2 bp	2.9	3.3	Round	23	11	14	_	_	_	_
P20	c.2961_2962insGGGGT; p.(Thr988GlyfsTer45)	5 bp	4.6	4.3	Linear	21	9	8	_	_	_	_
P21	c.3015_3032delinsTG; p.(Tyr1006AlafsTer20)	18 bp	13.5	4.5	Linear	18	6	4	_	_	_	_
P22	c.4365_4368del; p.(Ser1456CysfsTer4)	4 bp	3.6	3.5	Round	ND	ND	ND	_	_	_	_
P23	c.3989_4001del p.(Arg1330LeufsTer25)	13 bp	6.3	4.2	Linear	11	3	14	_	_	_	_

P24	c.3989_4001del; p.(Arg1330LeufsTer25)	13 bp	12.3	4.1	Linear	ND	ND	ND	_	_	_	_
P25	c.3891_3910del p.(Ser1297ArgfsTer67)	20 bp	3.5	3.9	Linear	26	11	19	_	_	_	_
P26	c.3904dupG p.(Ala1302GlyfsTer69)	1 bp	5.1	3.5	Round	ND	ND	ND	_	_	_	_
P27	c.3904dupG p.(Ala1302GlyfsTer69)	1 bp	2.5	3.6	Round	11	12	2	_	_	_	_
P28	c.3904dupG p.(Ala1302GlyfsTer69)	1 bp	5.6	3.9	Linear	28	14	6	_	_	_	_
P29	c.3904dupG p.(Ala1302GlyfsTer69)	1 bp	7.5	0.6	Round	ND	ND	ND	_	_	_	_
P30	c.3904dupG p.(Ala1302GlyfsTer69)	1 bp	16.0	4.1	Linear	29	9	17	_	_	_	_
P31	c.2101_2102dup p.(Gly702ArgfsTer8)	2 bp	17.0	2.6	Linear	14	13	8	_	_	_	_
P32	g.50684024_50739836del	55.8 kb	4.08	2.8	Linear	ND	ND	ND	_	_	_	_
P33	g.50706752_50739896del	33.1 kb	21.9	4	Round	ND	ND	ND	_	_	_	_
P34	g.50666057_50706931del	40.9 kb	8.0	2.1	Linear	13	4	5	_	_	_	_
P35	g.50684024_50714476del	30.5 kb	9.0	2.5	Linear	ND	ND	ND	_	_	_	_
P36	g.50684024_50739836del	55.8 kb	9.1	1.8	Linear	ND	ND	ND	_	_	_	_

SHANK3 sequence variants are annotated using the MANE Select transcript, NM_001372044.2. 22q13 deletions (GRCh38) are stratified into Class 1 and Class II. Class I deletions include only *SHANK3* or *SHANK3* in combination with ARSA, ACR and/or RABL2B. Class II deletions include all deletions that did not qualify as Class I deletions. Class II deletions were further stratified by size: d: < 4 Mb, D: ≥ 4 Mb. The size and shape of the forceps minor are indicated. The table also shows the Autism Diagnostic Interview-Revised (ADI-R) scores across domains: (A) social interaction, cut-off ≥ 10, (B) communication, with nonverbal cut-off ≥ 7, and (C) patterns of behaviors, cut-off ≥ 5. Radiological abnormalities identified in each patient are also described, including cortical atrophy, dysmorphic corpus callosum, septal cyst, cerebellar dysplasia, ectopic posterior pituitary, and abnormal temporal myelination. Mb, megabases; kb, kilobases; bp, base pairs.

Table 2. Brain regions showing ASL-MRI hypoperfusion in Phelan–McDermid syndrome patients with Class I deletions, Class II deletions and *SHANK3* sequence variants

Cluster number	Cluster size (voxels)	Peaks (x,y,z) (MNI)	Z-value	T-value	P_{FWE}
Bilateral temporal regions					
C1	103	57 -40 2	5.50	8.06	0.001
C2	61	69 -42 0	5.40	7.79	0.002
C3	210	-62 -6 -14	5.58	8.26	0.001
C4	73	-68 -38 0	5.20	7.29	0.006
Bilateral frontal regions					
C5	69	3 42 -16	5.00	6.84	0.014
C6	52	26 28 -20	5.21	7.32	0.006
C7	57	-34 40 -16	5.50	8.05	0.001
C8	83	-50 10 –3	5.52	8.12	0.001
Left mesial precentral gyrus					
C9	139	-2 -22 50	5.32	7.59	0.003
Left supramarginal gyrus					
C10	99	-66 -40 34	5.83	8.97	< 0.001

This table shows all clusters resulting from whole-brain voxel-wise Statistical Parametric Mapping (SPM) analysis of rest Cerebral Blood Flow(rCBF) in 7 patients carrying either class I deletions, class II deletions or sequence variants, compared to 21 age-matched controls, corrected for multiple comparisons using family-wise error (FWE). MNI, (Montreal Neurological Institute).

Figures

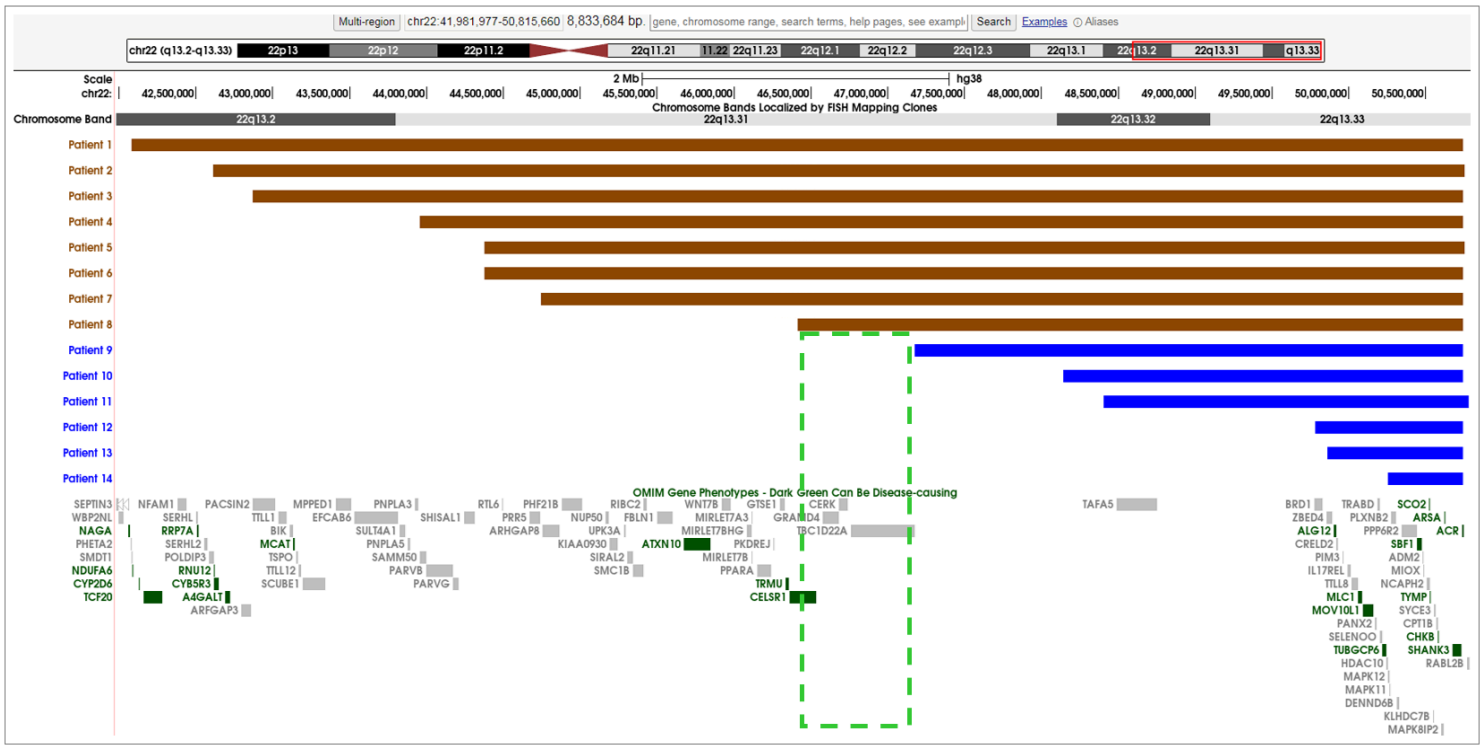


Figure 1

Mapping of 22q13.2–q13.33 deletions encompassing the *SHANK3*gene. Patients 1-15 are shown in descending order of deletion size. Chromosomal coordinates are based on the GRCh38 genome build. Patients presenting normal forceps minor are shown in blue. Patients with forceps minor anomalies are

shown in brown. Green dotted lines define the smallest region of overlap (see Table 1).

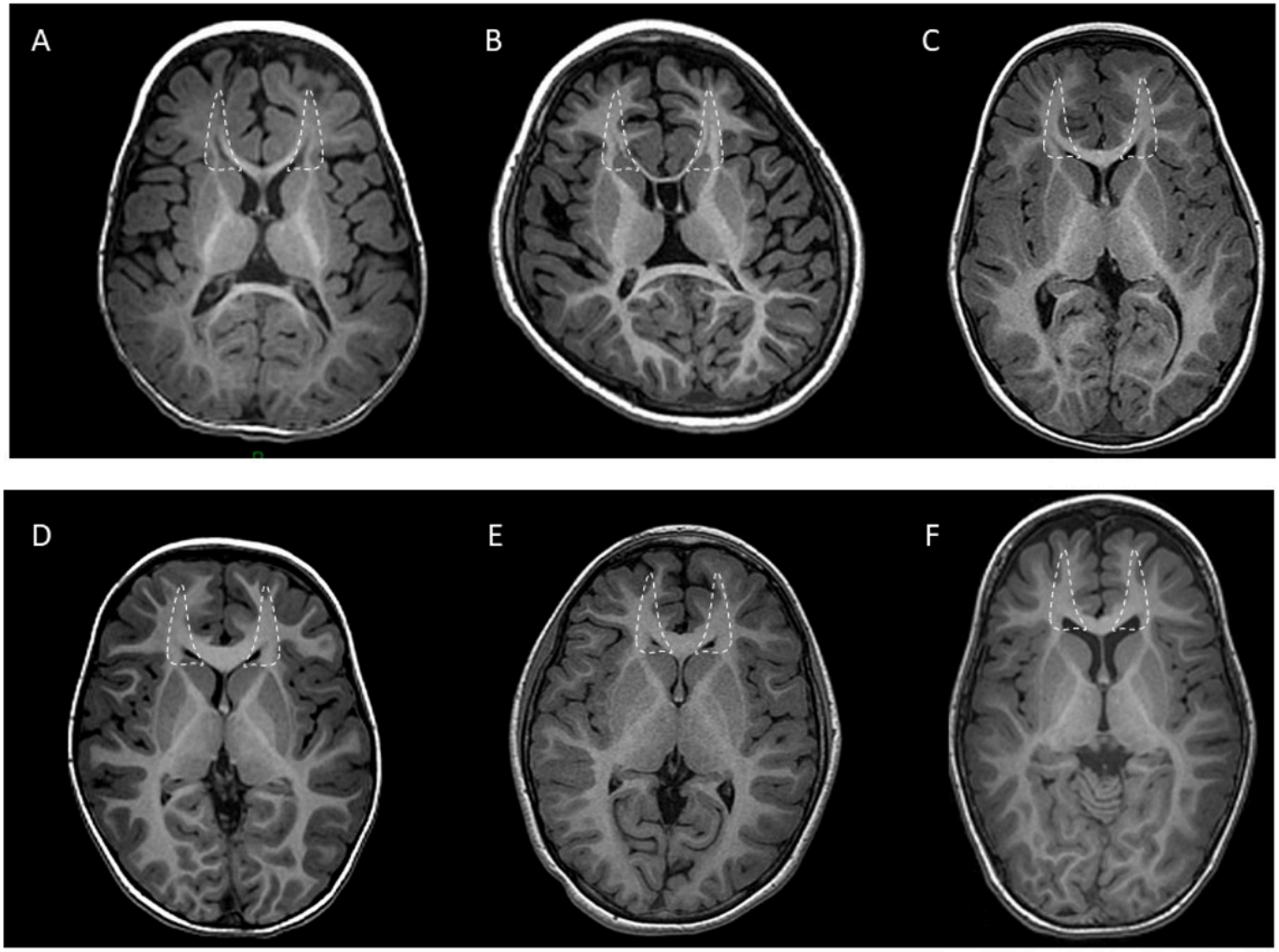


Figure 2

Forceps minor morphology assessed on axial T1-weighted MRI in patients with 22q13 deletions and *SHANK3* sequence variants.

Upper panel: Brain MRI of three children carrying large-scale Class II deletions (6–8.7 Mb). (A) 13-month-old patient (P6); (B) 2.6-year-old patient (P2); (C) 7.7-year-old patient (P5). On all axial T1-weighted images, the forceps minor appears as a hypointense, elongated structure (> 5mm), particularly visible at the level of the basal ganglia. Dotted lines indicate the location of the forceps minor.

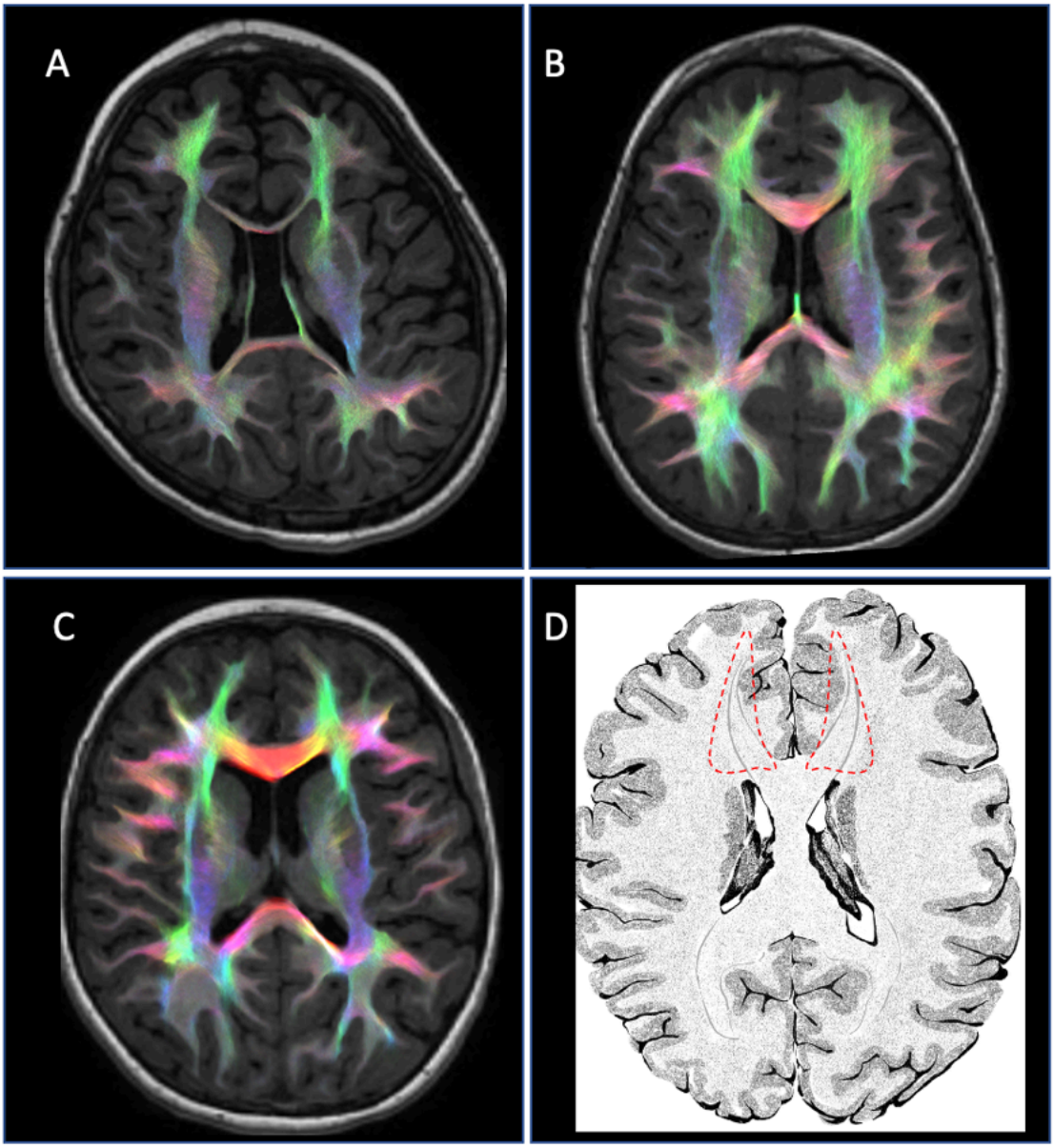


Figure 3

Diffusion MRI tractography illustrates of the forceps minor and corpus callosum in 22q13 Class II deletion, *SHANK3* sequence variants, and control. Representative fiber tractography reconstruction generated from diffusion- weighted MRI of the forceps minor and the corpus callosum region. of two 7-year-old patients carrying either a large-scale 22q13 deletion (A, patient P5) or a *SHANK3* sequence variant (B, patient P23) and (C): age-matched control. (A) The forceps minor and the corpus callosum region show a marked reduction in the number of white matter fibers. The forceps minor is abnormally elongated, rigid and dysmorphic. (B, C) Right and left fiber bundles of the forceps minor are normally symmetrical, with regular curvature and no deviation, flattening or asymmetry. (D) Schematic anatomical representation of forceps minor. Dots indicate the normal anatomical location of the forceps minor. Illustration by Ninon Chauveau, adapted from The Human Central Nervous System [41].

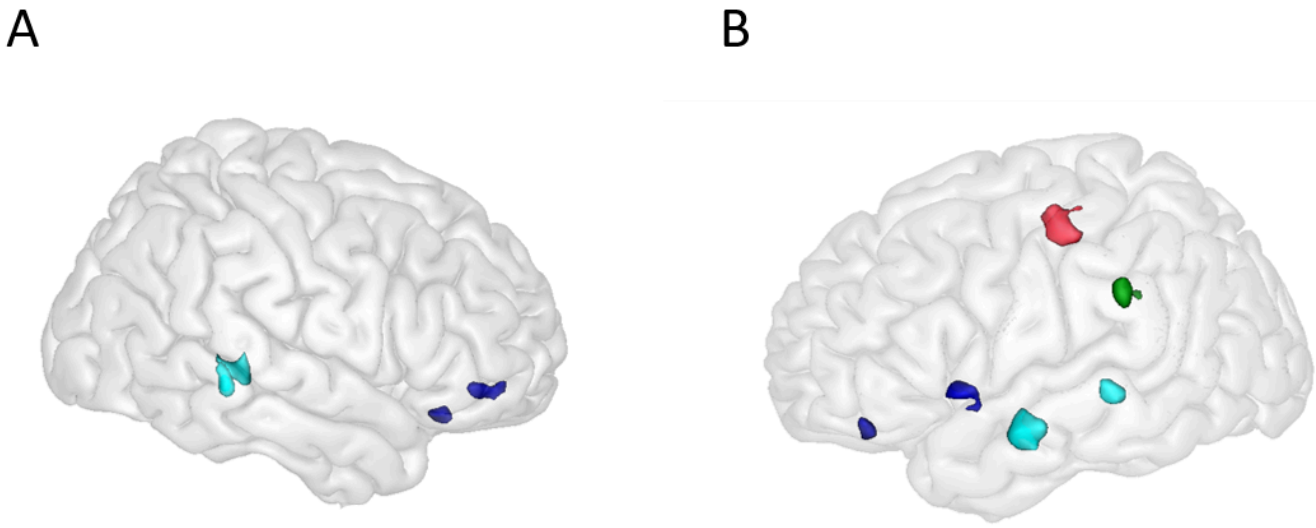


Figure 4

Significant clusters showing hypoperfusion in patients with 22q13 deletions and *SHANK3*sequence variants compared to age matched controls.

Whole brain voxel-by-voxel SPM analyses corrected for multiple comparisons, were performed on ASL perfusion data to compare 7 children carrying either Class I or II or *SHANK3*sequence variants and 21 age matched controls. All the significant clusters from table 2 are shown, projected onto a transparent 3D anatomical brain template on sagittal view. Figure A represents the right hemisphere, showing two temporal clusters in turquoise (C1–C2) and two frontal clusters in dark blue (C5–C6). Figure B: represents the left hemisphere, showing two temporal clusters in turquoise (C3–C4) and two frontal clusters in dark blue (C7–C8). The left mesial precentral gyrus cluster (C9) is shown in red, and the left supramarginal cluster (C10) is shown in green.